Investigation of surface integrity in laser-assisted machining of nickel based superalloy

Xu, D., Liao, Z., Axinte, D., (...), M'Saoubi, R., Wretland, A.

University of Nottingham Ningbo China, 199 Taikang East Road, Ningbo, 315100, China

First published 2020
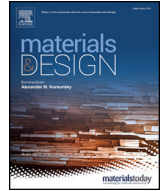
Investigation of surface integrity in laser-assisted machining of nickel based superalloy

Dongdong Xu [a], Zhirong Liao [a,*], Dragos Axinte [a,b,**], Jon Ander Sarasua [c], Rachid M'Saoubi [d], Anders Wretland [e]

[a] Machining and Condition Monitoring Group, Faculty of Engineering, University of Nottingham, Nottingham, UK
[b] Faculty of Science and Engineering, University of Nottingham Ningbo, Ningbo, China
[c] IK4-TEKNIKER, Eibar, Guipuzcoa, Spain
[d] Seco Tools AB, R&D Material and Technology Development, Fagersta, Sweden
[e] GKN Aerospace Engine Systems AB, Trollhättan, Sweden

HIGHLIGHTS

- This study reveals the machining mechanism of the laser assisted milling (LAMill) of nickel-based superalloy
- The LAMill machined workpiece presents less damage in reference to grain alternation (white layer and material drag)
- This study reveals the complex residual stress distribution in LAMill machined workpiece and its formation mechanism
- LAMill presents a potential for roughing machining but a subsequent finishing or post-process is recommended

GRAPHICAL ABSTRACT
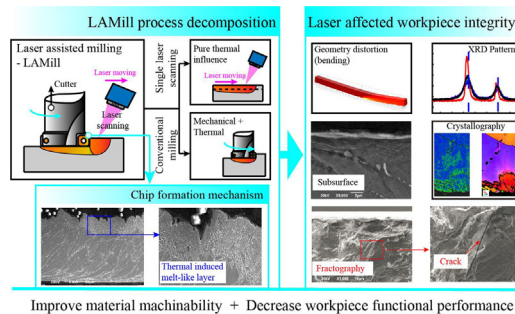
ABSTRACT

While laser-assisted machining can significantly improve the machinability of nickel-based superalloy, the mechanism of surface integrity evolution and its influence on the material functional performance is still not clear. The present study gives a comprehensive investigation on the surface integrity of laser-assisted milling (LAMill) process with an in-depth study of the mechanism of chip formation, microstructural and mechanical alternations, supported by key outcomes from the two constitutive processes, conventional milling (CMill) and single laser scanning (LS). Although the high thermal affected layer in LAMill process has been removed through the cutting chips, a significant bending effect has been found in both the LAMill and LS workpiece. More interestingly, a combined impact of the residual stress from LS and CMill has been found on LAMill workpiece while a lattice evolution has been revealed regarding both the thermal and mechanical influence. Specifically, inadequate fatigue performance on LAMill and LS workpiece has been found due to the high thermal effect in the superficial layer regarding the residual tensile stress distribution and microstructure variation. While LAMill is generally considered as a promising machining method with improved machinability of difficult-to-cut materials, this research shows a poor workpiece functional performance (fatigue) and justifies its application prospect.

* Corresponding author.
** Correspondence to: D. Axinte, Faculty of Science and Engineering, University of Nottingham Ningbo, Ningbo, China.
E-mail addresses: Zhirong.Liao@nottingham.ac.uk (Z. Liao), Dragos.Axinte@nottingham.ac.uk (D. Axinte).

1. Introduction

High-strength materials (e.g. Ni/Ti-based superalloys) are widely used in the value-added industries such as aerospace, nuclear and medical sectors because of their superior thermo-mechanical characteristics (e.g. high temperature and corrosion resistance) that keep the manufactured component operating stably even in harsh working environments [1–3]. However, their unique properties, such as low thermal conductivity [4], high strength at elevated temperature [5] and work hardening [6], lead to high machining difficulties (e.g. significant tool wear, unfavourable workpiece surface integrity and low material removal rates) [7]. To improve the machinability of these difficult-to-cut materials, thermally-assisted machining (TAM) methods, have been proposed to locally preheat the workpiece ahead of the cutter and thus, to soften the material at elevated temperature [8–10]. Laser-assisted machining (LAM), as a classical representative of TAM methods, has the advantages of reducing cutting force [11], suppressing chatter [12], improving productivity [13] and enabling longer tool life [14]; thus, it has been considered as a promising process to improve the machinability of difficult-to-cut materials while attracting significant attention from academic and industrial communities.

Currently, LAM is mainly employed on either turning or milling process, whereby a single laser spot is usually placed ahead of the cutter as the heat source, to validate the effectiveness of LAM methods [15–18]. However, the difficulty to heat the workpiece homogeneously, e.g. which is limited by the laser spot size when compared with cutting width, leads to poor machining effect (e.g. partially over or under heated workpiece) and significantly restricts the practical application of LAM. To solve this problem, recently a heat placement control method regarding both forward and inverse problems in LAM milling process has been proposed [19], which enables heating a large workpiece volume ahead of the cutting edge in a homogeneous manner by using a relatively small laser spot size (Fig. 1). The results show that this smart strategy of moving the laser beam process could significantly reduce the cutting forces and improve the material removal rate when laser-assisted milling of Inconel 718.

Nevertheless, while the LAM method has been proved beneficial for improving the machinability of difficult-to-cut materials, it is not clear how LAM process would affect the surface integrity and eventually the functional performance of these machined components, especially considering the included high thermal energy. Specifically, for those components used for safety-critical applications (e.g. aero-engine or nuclear plant), surface integrity is crucial to their service performance. Consequently, there is the open question if the surface integrity and mechanical performance (e.g. fatigue life) of workpiece generated by LAM process are good enough for the industrial applications despite its advantages in improving machinability.

In general, it is believed that in the LAMill process the extra thermally affected layer (by the laser beam) in the workpiece will be removed with the cutting chips through the follow-up material removal process (Fig. 1a) [11]. However, due to specifics of Nickel-based superalloys, i.e. nearly constant strength under a critical high-temperature region, to soften the surface layer in LAMill process significant and uniform heating of the workpiece is needed in a well-defined volume. In these conditions, although only the materials in to-be-removed areas (cutting depth) have been softened, the materials under this area will be heated up as well; thus, a certain amount of heat and residual thermal load will still penetrate into the bulk material. Thus, combined with the mechanical effect from the machining process itself, LAMill would introduce a particular residual stress distribution, while the combined effect may also alter the microstructure of the machined workpiece. This combination of the thermal and mechanical effects may, eventually, influence the functional performance of the workpiece material, such as fatigue life, corrosion resistance, and static strength of machined components. However, up to date, the most relevant studies are either focusing on finite element simulation of LAM process (e.g. machining Inconel 718 [20]) to prove the effectiveness of LAM or modelling the generated residual stress on the laser-assisted workpiece [21] rather than a detailed investigation of the machined surface integrity and its functional performance. Indeed, the tool wear mechanism is also of importance in LAMill process because of the additional thermal influence; however, there are already quite a lot of publications investigated on this, e.g. [13,16,22]. Hence, while the surface integrity is more crucial to the safety-critical components, there is a lack of in-depth investigation on the workpiece surface integrity obtained by LAMill. Therefore the motivation of the present paper is to comprehensively reveal LAMill process and the microstructural alterations of materials and their influences on the functional performance.

2. Aims and research concept

To understand the mechanisms by which LAMill influence upon machined surface integrity and its functional performance, this research investigate the workpiece surface integrity resulting from three different processes, including controlled laser-assisted milling (LAMill) [19], conventional milling (with coolant) and single laser scanning. The chips formation from both LAMill and CMill process were studied to investigate the mechanism of surface generation through the combination of laser softening and mechanical cutting while the workpiece morphology has also been analysed to present the penetration of thermal loading from the laser softening. To reveal the microstructural and lattice alternation in the superficial layer, an in-depth study of the machined workpiece was conducted by employing both the electron backscatter diffraction (EBSD) microscope and X-ray diffraction (XRD) techniques.
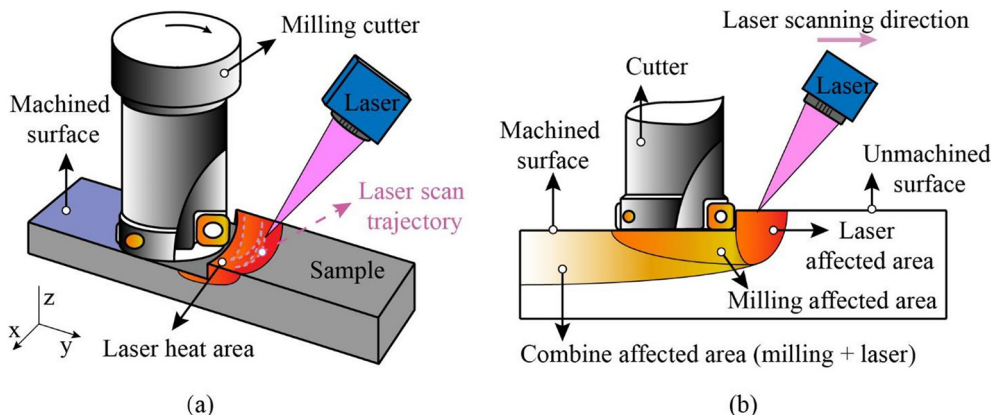

Fig. 1. Heating effect of Laser-assisted milling (LAMill) process. Laser scanning trajectory for uniformly 3D heating the workpiece (a); and heat influenced superficial layer (b).

The functional performance of machined workpiece was also investigated by carrying out fatigue tests and fracture analysis proving that the LAMill process yields an inadequate functional performance due to the residual thermal effect and post-process is needed. The present study exhaustively reveals the LAMill generated workpiece, allowing the manufacturing community to progress the application of LAM and put in place post-processing methods for surface quality enhancements to enable the adequate functional performance of the components.

As schematically indicated in Fig. 2a, the LAMill process involves a complex loading (including laser heat, cut heat and mechanical loading effect) on the machined workpiece, leading to compound surface integrity (e.g. the residual stress distribution – RS1 is a combination of RS2 and RS3). However, as shown in Fig. 2, the LAMill process can be considered as the combination of pure laser scanning- LS (Fig. 2b) and conventional milling-CMill (Fig. 2c), which gives the possibility to study the influence of three different processes independently and compared again later. In general, the single laser scanning (LS) process only induces a tensile thermal effect (Fig. 2b) on the workpiece, while the conventional milling (CMill) would introduce a compressive mechanical effect to the machined workpiece (Fig. 2c) if not under high cutting temperature. As a consequence, the impact from CMill and influence of LS on machined surface integrity can be investigated separately to support the understanding of workpiece surface integrity evolution when the laser is introduced into the mechanical cutting process, i.e. LAMill.

3. Experimental methodology

In this study, a 5-axis milling machine tool integrated with a 10 kW diode laser system (laser spot diameter is 3 mm) is employed for the experimental study, as shown in Fig. 3 (a). The LAMill process was carried out based on an established inverse control method [19], whereby a path-optimised trajectory with the varied laser power (1300w, 1400w and 1500w) and scanning speed of 300 mm/s was applied to achieve a homogeneously distributed heat affected zone in front of the milling cutter and cover whole cutting width area. It is worth to note that the detailed explanation of LAMilling cutting parameters selection and optimization can be found in previous study [19]. A milling cutter (SECO high feed mill R217.21-3232.0-LP06.4A) with a diameter of 32 mm was employed for end-milling of Inconel 718 samples with dimensions of 125 mm × 6.5 mm × 6 mm, as shown in Fig. 3 (b). To decompose the LAMill process, another two processes (conventional milling without laser, and pure laser scanning on the sample without material removal) are presented as comparison, in which the adopted cutting parameters can be found in Table 1. The laser scanning parameters for LS process are

the same as LAMill while the CMill is applied with supplying cutting fluid at 50 bar to make comparison with the conventional approach.

The machined workpiece has been analysed by using surface topography measurement (Alicona InfiniteFocus and MountMap) while scanning electron microscope (SEM: JEOL 6490LV) and electron backscatter diffraction (EBSD: Oxford Instrument NordlysMax3) techniques ae employed to evaluate the microstructure variation in the superficial layer. A Proto iXRD machine with a 2 mm diameter aperture and 12.5 kV voltage is applied for residual stress profile measurement to a maximum depth of 1200 μm under the machined workpiece surface by using electropolishing. To reveal the microstructure properties on the surface of machined workpieces, X-Ray diffraction diagrams are also acquired with Bruker D8 Advance with DaVinci X-ray Diffractometer.

In order to investigate the surface integrity influence upon the functional performance of the workpiece machined in different processes, a four-point bending fatigue test was employed on a closed-loop servo-hydraulic testing machine (Instron 8801) (Fig. 4). Sinusoidal cycles (stress ratio $Stress_{min}/Stress_{max} = 0.1$) have been run at room temperature in constant load mode with specific loading conditions as 100% and 10% of the yield stress (1250 MPa), as shown in Fig. 4b. It is worth to mention that the LAMilling process with 1400w laser power is taken as an example to study the thermal influence regarding geometry bending, chip characterisation changing, microstructure alternation as well as fatigue performance; however, the influence of thermal from applied three different laser power are presented in the workpiece residual stress distribution.

4. Laser thermal field induced workpiece distortions

As the basic theory of LAMill relies on applying additional thermal to soften the materials, naturally, the workpiece stress state will be influenced and thus, prone to alter the geometry of machined components especially for thin parts (e.g. the one used in the present study) of "open geometries". What is meant by this: if the part is of a "closed geometry", e.g. cylinder, the stresses induced by the additional thermal field (that moves around the circumference) are likely to be redistributed and, hence limited geometrical distortions are expected. Nevertheless, in the case of the current research, to enable the preparation of fatigue samples (required to be at high geometrical accuracy) a special manufacturing procedure worth to be designed. To study the thermal influence on current "open geometries" samples, the LAMill machined workpiece geometry deviation has been measured by Alicona 3D scanning, while LS and CMill workpiece is taken as a comparison. Single extract profiles sectioned
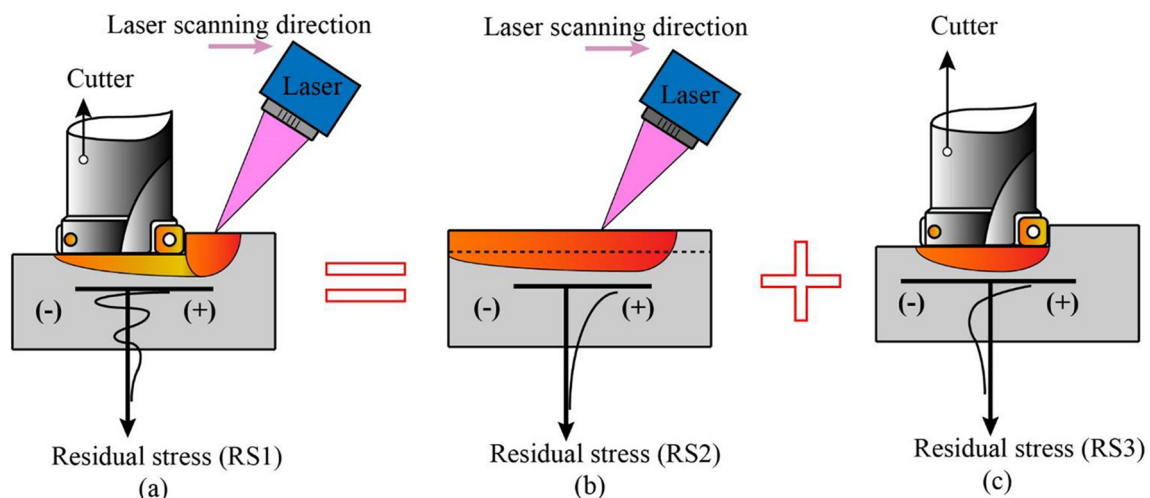

Fig. 2. Illustration of the "decomposition" of laser-assisted milling process (a) into laser scanning (b) and conventional milling (c) from residual stresses distribution of perspective.
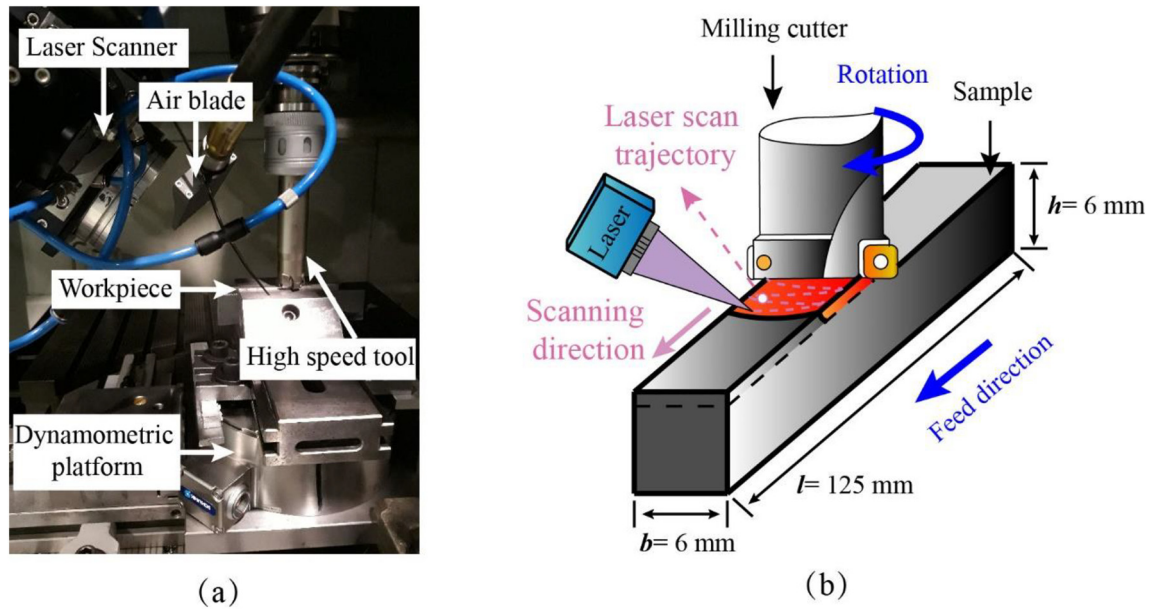
Fig. 3. Employed laser equipment on a milling machine (a) and schematic of the setup (b).

Table 1
Specification of the experimental tests.

Test description	Laser-assisted milling (LAMill)	Laser scanning (LS)	Conventional milling (CMill)
Laser power (W)	1300, 1400, 1500	1300, 1400, 1500	–
Laser scanning speed(mm/s)	300	300	–
Cutting speed (m/min)	45	–	45
Cutting depth (mm)	0.25	–	0.25
Cutting width (mm)	6	–	6
Federate (mm/tooth)	0.25	–	0.25

following the cutting direction of the workpiece are presented to show the generated surface curve from different process methods.

As expected, the test piece in LAMill (Fig. 5a) presents a geometry deviation (in this case: bowing at large radius, 5342 mm, which is a maximum vertical difference of 310 μm) although it is believed that the main heat softened material has been removed through the hybrid machining process generated chips. In further, as a comparison, the CMill manufactured workpiece presents a relatively flat surface (Fig. 5b) with the surface profile variation in the range of around 50 μm in the vertical direction. Not surprisingly, the laser-scanned (LS) workpiece, which is introduced to understand the influence of laser sources on deformation, shows a more significant bending (Fig. 5c), that an arc profile with a radius of 3076 mm can be identified.

The results show that the extra thermal loading in the LAMill process leads to the obvious workpiece bending as well compared with the CMill process, while this bending effect is smaller than the LS process. This is because, on the one hand, the machining process in LAMill has removed a layer of thermal affected material (in this case, 250 μm), while on the other hand, apart from thermal loading the machining process also brings mechanical compression on the workpiece, which will compensate the thermal bending effect. Compared with the workpiece from CMill machining process where only machining generated heat is involved, the LAMill and LS process has brought significant additional heat and left a considerable amount of thermal stress into the workpiece, leading to an evident bending effect on the workpiece.
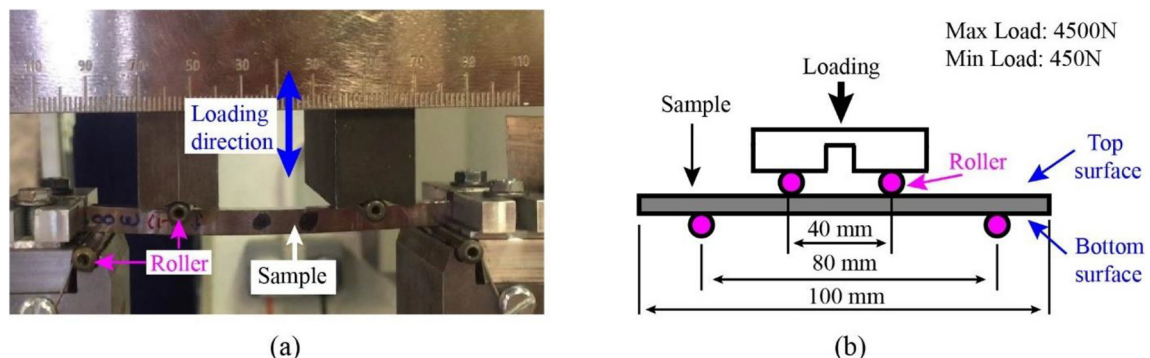

Fig. 4. Experimental setup for fatigue testing (a) and illustration of the loading arrangement (b).

To further understand the mechanism of introduced laser's influence on machined workpiece geometry, numerical modelling of the additional thermal loading introduced by laser scanning on the present workpiece in the time domain is scarried out (COMSOL Multiphysics) with both heat transfer, and solid mechanics module included. The laser is modelled as a Gaussian heat moving source that runs at the top surface of the workpiece, which is similar to the pure laser scanning. For the present simulation definition, the main description of the heat is presented and the analytic functions of moving heat source could be expressed as shown in Eq.1 [23,24].

$$q_s(y,t) = e^{\dfrac{-\left[y-\left(v_c \cdot t - \dfrac{L}{2}\right)\right]^2}{(2 \cdot r)^2}} \tag{1}$$

Where q_s is the moving the heat source; v_c is the feed rate of laser (800 mm/min); L is the sample length (125 mm); r is the radius of Gaussian source (1.5 mm); y is the displacement (unit: m) and t is the time (unit: s).

The top surface heat could be given by the following equation [24]:

$$-\boldsymbol{n} \cdot \boldsymbol{q} = q_0 \tag{2}$$

Where q_0 can be determined by the heat rate in Eq.3 and Eq.4. While $\boldsymbol{q}$ can be determined by Eq.5 [24] and $\boldsymbol{n}$ is the normal vector to the surface.

$$q_0 = \frac{P_0}{A} \tag{3}$$

$$P_0 = P_{in} \cdot m \cdot q_{(y,t)}; (t \leq 10s) \tag{4}$$

In which, P_{in} is the laser power (1750 W); m is the absorptivity factor (4); A is the surface area of the surface-emitting heat.

$$\boldsymbol{q} = -k \cdot \nabla T \tag{5}$$

Here, $\boldsymbol{q}$ is the heat flux, k is the thermal conductivity and ∇T is the temperature gradient.

The cooling condition is set as externa natural air convection, and T_{room} (room temperature) is 20 °C and it following Eq.6.

$$q_0 = h \cdot (T_{room} - T) \tag{6}$$

Where h is the heat transfer coefficient, and T is the real-time temperature.

As seen the simulated results in the time domain, the sample starts to slightly bend at the laser-scan heated area on the left end of the sample in Fig. 6a, but in a downward direction, while the non-scanned area keeps steady. The thermal expansion causes a distinct bending of the sample (Fig. 6b) at the time of 5 s when the laser scans to the middle of the workpiece but both ends of the sample bend to the downward direction. As a comparison, after the sample cooled down to a low temperature (<200 °C), the workpiece bend to the upward direction (Fig. 6c) which is caused by the residual stress generated from the thermal effect in the LS process, explaining the severe plastic distortion appearance on the LS sample (Fig. 5c). As seen in Fig. 6d, the contours of deformed workpiece showing a bending curve with a radius of 3520 mm (maximum height difference: 360 μm), which is consistent with the measured LS experimental results ($R = 3076$ mm).
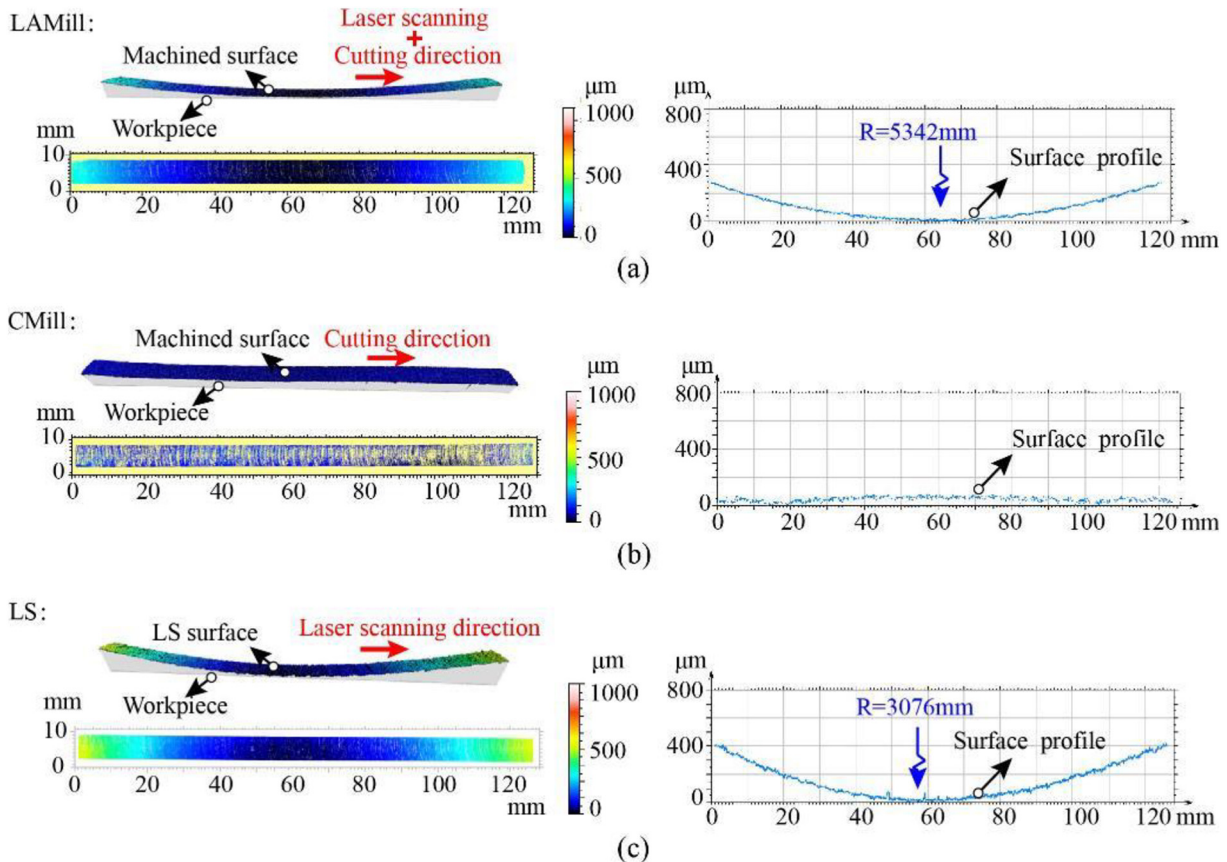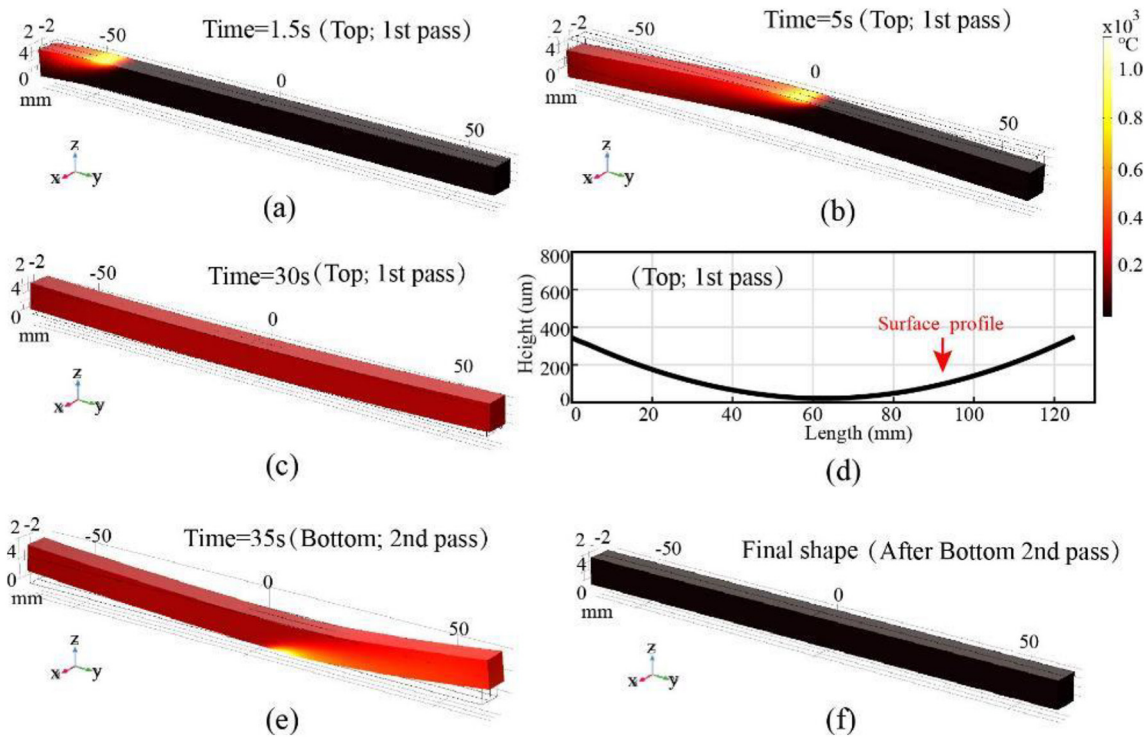

Fig. 5. Examples of measured macro and micro geometries of the test pieces resulting from LAMill (a), CMill (b), and LS (c).

Fig. 6. Simulated sample bending caused by laser scanning: 1st pass and $t = 1.5$ s (a); 1st pass and $t = 5$ s (b); and 1st pass and $t = 30$s (c); the surface profile of workpiece in a section at the length direction after 1st pass at t = 30s (d); 2nd pass and t = 35 s (e); and final shape after 2nd pass process on the bottom surface (f).

To avoid the irregular geometry generated in LS and LAMill pro- cesses and acquire relative flat samples for carrying out fatigue tests, an- other pass of laser scanning is applied on the opposite surface of the sample (Fig. 6e), and the simulated final sample geometry is presented (Fig. 6f), showing a flat surface. Therefore, all of three kinds of samples (LAMill, LS and CMill) for fatigue tests are processed with the machining on both top and bottom surfaces as illustrated in Fig. 7 (taking LAMill as an example), where the sample is rotated upside down after the 1st pass and carried out the 2nd pass for compensation. It is worth to note that after this procedure, geometry deviations (bending) of all samples are kept in the range of 50 μm, which is suitable for fatigue tests.

5. Results and discussions

5.1. Morphology and microstructural analysis of chip

Evidently, the chip generation of LAMill will display significant dif- ference with the CMill ones as the introduced laser is supposed to ho- mogeneously soften the materials to be removed and forming chips later (Fig. 8a). Therefore, it is worth to study the characteristics of the

generated chips, which play important roles in the machining process, to understand the influence of employed laser on the milling process and then surface integrity. As seen from Fig. 8b, it shows the chip evolu- tion process in LAMill, while the generated serrated chips and heated area by laser are indicated. To fully present the milling generated chip characteristics and investigate the material alternation of chips in detail, the generated chips were sectioned as section A (along with the chip height – see the green plane in Fig. 8b) and section B (along with the chip length - see the yellow plane in Fig. 8b). The section views (Fig. 8c) illustrate the definition of different areas on the generated chips: chip back surface (CBS) is the area contacting with tool rake face, chip free surface (CFS) is the laser-scanned area, and chip top sur- face (CTS) is the serrated surface of the chip. Chips from both LAMill and CMill have been studied following the described method.

The LAMill generated chips present 2.5 times larger section area (Fig. 9a: 3.1 mm in length and maximum 360 μm thickness) than the CMill ones (Fig. 9b: 2.2 mm in length and maximum 234 μm thickness), which is because the softened materials can be compressed more. To understand the influence of introduced laser on chip's microstructures, SEM observations with higher magnification on both chip free and back
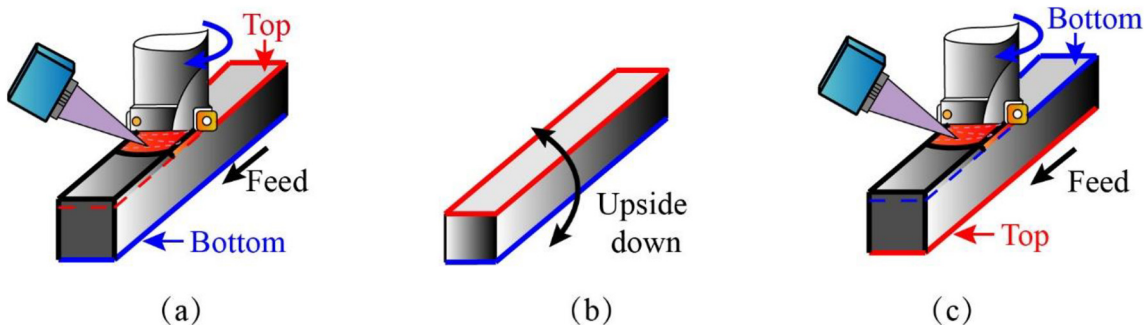
Fig. 7. Preparation of the fatigue samples by LAMill to avoid distortions: 1st pass process on the top surface (a); upside-down rotation of the machined sample (b); and 2nd pass process on the original bottom surface (c).
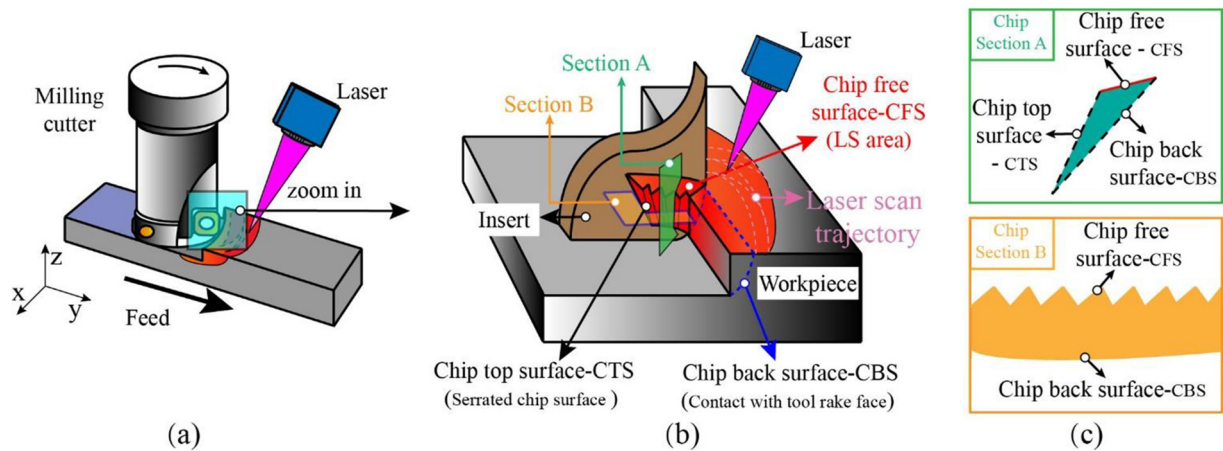
Fig. 8. Illustration of the generated chips in milling and the corresponding sections to reveal the properties of the chip: Overview of LAMill process (a); enlarged image of the chip generation area (b), and associated cross sections A and B (c).

surface are implemented. As seen, the free surface (CFS) of LAMill chip (Fig. 9c) shows that the material on the uncut top surface has been heated to a high temperature which leads to a melt-like layer near the free surface area; in contrast, on the CMill chip (Fig. 9d) no evident thermal effect is observed. More interestingly, while the cutting force of LAMill process is smaller than CMill [19], a more severe deformed chip has been observed in LAMill. This is due to the lower material strength, and young modulus has been achieved by the thermal effect induced by the laser [25,26] which leads to a thicker chip thickness from chip compression effect. A smoother surface is presented on the LAMill chips (Fig. 9e), while denser crystal slips, which is believed to be caused by higher cutting force and friction effect when machining by CMill [19], can be identified in the CMill generated chips (Fig. 9f).

Seen from B section view (Fig. 10a), a melt-like layer on the chip free surface (CFS) by has been observed (Fig. 10c) on LAMill chip; this is in correlation to the findings in the section A of the chip (see Fig. 9c). As a comparison, clear sharp teeth can be seen from the CMill chips, and apparent dense shear bands (Fig. 10d and f) have been observed which are correlated to the crystal slips in Fig. 9d and f. More interestingly, at the back surface, LAMill generated chip (Fig. 10e) displays a smooth material deformation with no slip bands, indicating a deformation under the soft condition of the material. However, a severely deformed layer (Fig. 10f), including white layer and massive slip bands, is generated at the back surface areas of the CMill chip, which, as known, results from the significant friction between tool rake face and chips. These phenomena can be apparently explained that the material in the LAMill process is softened, therefore less normal force is applied on the tool rake face, which leads to less friction and shear deformation, while the opposite for CMill.

As presented, the generated chips with and without assisted laser show the significant difference that the LAMill chip becomes considerably thicker because of the easier compression of soft materials; the chips free surface indicates melt-like layer, and it expresses less serve deformation (less crystal slip bands dense). These phenomena indicate the influence of additional laser on the chips shapes and microstructures; thus, it is reasonable to assume that the laser has undoubtedly brought an impact on machined workpiece surface integrity. The further in-depth understanding of the surface generation and material microstructural evolution will also be investigated in the following sections with state-of-art methods.

5.2. Microstructural analysis of the workpiece surface integrity

Surprisingly, the surface integrity in microstructure view of LAMill machined workpiece shows no evident grain deformation (Fig. 11a), where only a thin white layer (0.5 μm thick) can be noticed in Fig. 11

(b). In contrast, a clear continuous white layer (~2 μm thickness) accompanied by a 4 μm material drag layer (Fig. 11d) is found in the superficial layer of CMill workpiece, indicating a severe plastic deformation (SPD) of materials in this process. From the point of view of grain alternation (white layer) and deformation (material drag), LAMill process presents a less distinct variation on the machined surface comparing with the CMill generated workpiece, which might be because we controlled the heat flux to be distributed homogenously by optimizing the laser scanning trajectory [19]. Interestingly, in LS workpiece a grain refinement layer with clear small crystals is observed in the subsurface (Fig. 11e and f) due to the significant thermal loading on the workpiece which leads to materials melting and re-solidification (the detailed thermal distribution can be found in [19]). This evenly distributed small grains prove the effectiveness of selected LAMill parameters to homogenously heat up the un-cut materials by the inverse problem. In the LAMill process, while this re-solidification layer will be removed with the chips, and it can be related to the melt-like layer observed on the chips (Fig. 9c and Fig. 10c). Nevertheless, the crystal morphology of this re-solidified layer (Fig. 11f), showing the material softening effect induced by the laser without mechanical loading, is clearly different from the CMill process generated white layer (Fig. 11b) which is caused by mechanical-thermal loading together and appears as featureless and white. The results show the significant discrepancy on the surface microstructure alteration due to the different cutting/surface modification mechanism of these processes in LAMill, CMill and LS processes (Fig. 11).

Further investigations of the crystal structures with EBSD measurement reveals the impact on the grain morphology as a result of LAMill, in which both inverse pole figure (IPF) and band contract (BC) maps are presented (Fig. 12). There are no refined grains observed in LAMill surface (Fig. 12a and d) but small plastic deformation since the thermally refined grains by the laser have been removed by the milling process, which is consistent with above SEM observation. Moreover, as a comparison, a much deeper grain plastic deformation layer (Fig. 12b and e) has been observed in CMill sample when compared with the LAMill one due to the high cutting force in the conventional machining process, showing good correlation with the former analysis. As expected, the refined grains on the sample processed with LS could be clearly identified from the IPF map (Fig. 12c) and the clear grain boundaries in Fig. 12f. This can validate the influence of laser scanning (thermal loading) on the variation of the grain structure in superficial layer caused by re-solidification as found in the SEM images of chips (Fig. 9d) and surface (Fig. 11f).

To further understand the plastic strain distribution, the intragranular local misorientation (LMO) is measured (small orientation changes in the lattice under 5° subgrain angle) presenting the dislocations accumulated in the crystal during grain deformation, as shown in Fig. 13. From the
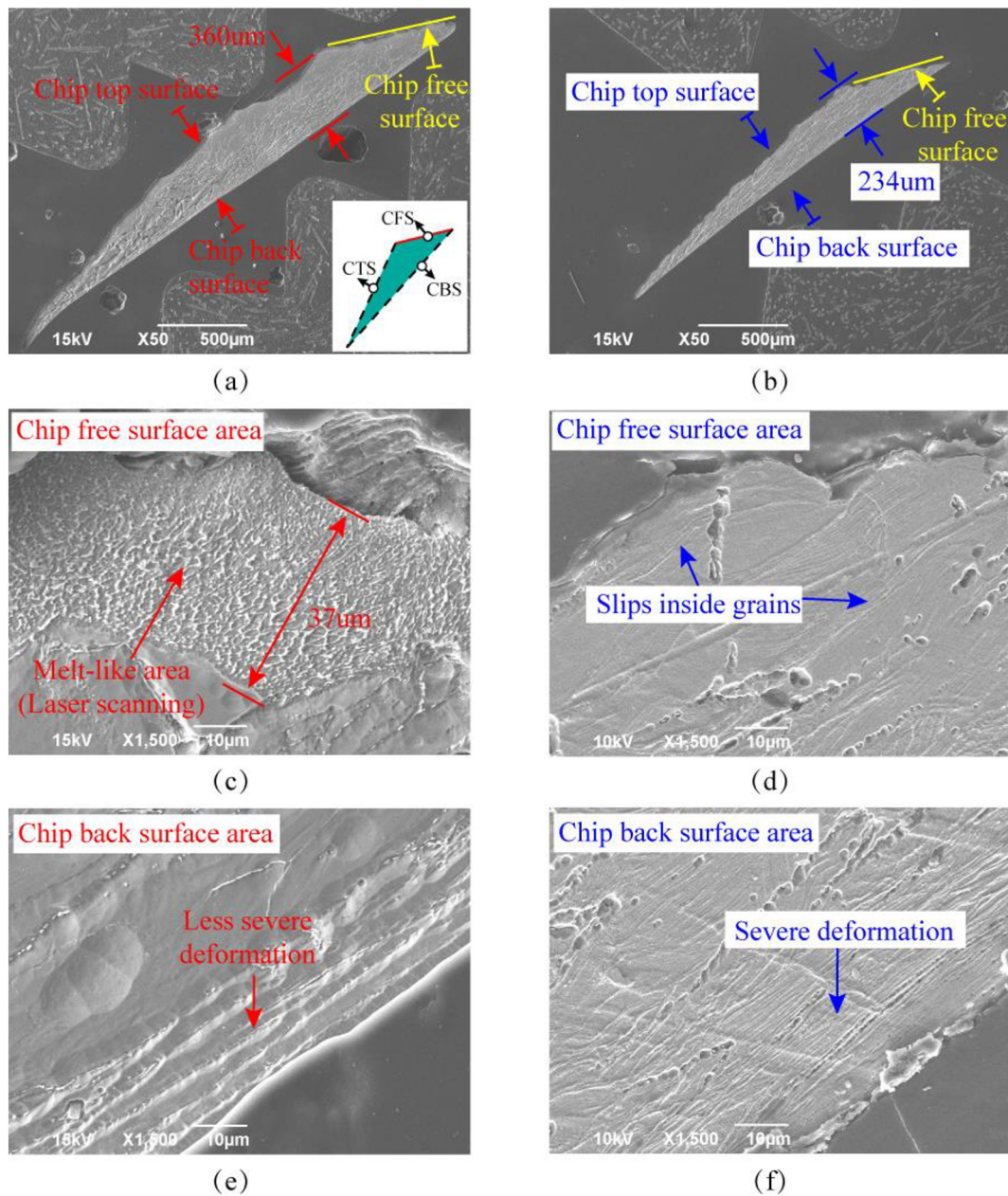
Fig. 9. SEM images of chips from LAMill and CMill process observed in cross section A: Images for LAMill process in different amplification and areas - (a), (c) and (e); images for CMill process in different amplification and areas - (b), (d) and (f).

LMO map, it can be seen that several strip-like aggregations of the misorientation (Fig. 13a), which are considered as the slip bands that consisted of several slip planes, were observed in LAMill samples and can be verified from the BC map in Fig. 12; in contrast, the CMill sample (Fig. 13b) displays clearer misorientation. Furthermore, the LMO contouring in the superficial layer of LAMill workpiece (Fig. 13a) shows less density while the CMill sample shows more LMO in a deeper area (Fig. 13b); although both of them present the concentrated LMO in the near-surface indicating the severe mechanical loading from milling. No doubt, in the LS samples (Fig. 13c), there is no clear misorientation in the superficial areas, indicating less mechanical deformation influence while the thermal strain cannot be quantified. This is because the local orientation alternation results from the generation and accumulation of dislocations during metal's mechanical plastic deformation, while the LS process only brings thermal loading on the sample and no mechanical loading is involved.

As a summary, less severe deformation (white layer and material drag) is found on LAMill machined workpiece, which is likely caused by

material softening induced by the laser beam ahead of a milling cutter with a secondary outcome of lowering cutting forces (validated in [14]); thus, LAMill results in less superficial surface microstructure alternation of the workpiece. The smaller grains on the near-surface area on LS processed workpiece presented by both the SEM and EBSD indicate that the top surface layer has been heated by laser to an extremely high temperature which even leads to the grain refinement. This re-solidification phenomenon can also be backed up by the melt-like layer in LAMill generated chips, which has been removed during the milling process. In addition, the even distribution of grain in the re-solidified layer proves the effectiveness of the proposed LAMill solution by the inverse problem.

5.3. Analysis of mechanical properties of the workpiece surfaces generated by different processes

As hybridisation of mechanical machining and laser heating processes, a unique residual stress profile in superficial areas from LAMill
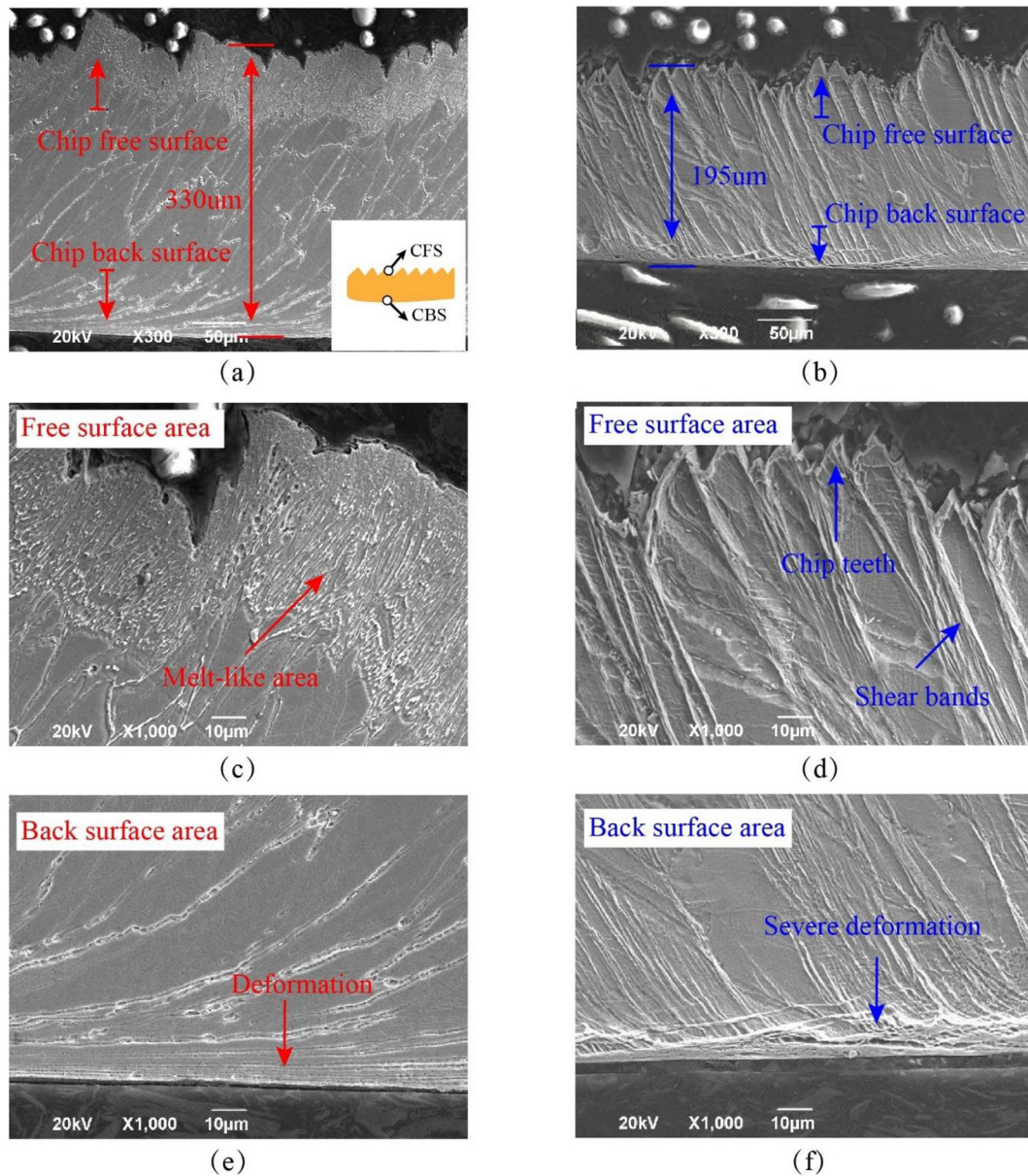
Fig. 10. SEM images of chips from LAMill and CMill process observed in cross-section B: Images for LAMill of different magnifications and areas - (a), (c), and (e); images for CMill - (b), (d), and (f).

workpiece can be found on the machined samples, as shown in Fig. 14 (a) and (b). Specifically, a thermally induced tensile stress from laser heating is found on the top surface (e.g. 1100 MPa at 1500 W) before a rapid decrease to 0 MPa at a depth of 100 μm, showing a compressive effect induced by the mechanical loading. Surprisingly, after the convergence to compressive state, the stress once again raises to a high tensile state whereby a maximum 1100 MPa is reached at a depth of around 400 μm under 1500w before it slowly decreases to the stress-free state at a depth of 1000 μm. In contrast, the CMill generated workpiece (Fig. 14c) results in tensile stress on the top surface (e.g. 431 MPa in feed direction) due to the high cutting temperature [27] while the stress rapidly decreases due to the mechanical effect when it goes deeper below free surface and goes back to the steady condition at around 320 μm depth in bulk materials. These residual stress results resulting from CMill show a common distribution which has been previously reported in the published literature [28,29].

Regarding the LS processed surfaces at various laser powers (1300 W, 1400 W and 1500 W), the residual stresses are in a tensile state to a depth of >400 μm when the stress becomes stable approaching the bulk state. At the same time, the higher laser power leads to a slightly more profound influence, as shown in Fig. 14 (e). It is not surprising that the tensile stress, which results from the significant thermal influence of laser heating on the surface, is much higher than the one in the CMill condition. It is interesting to notice that the residual stress profiles of LS generated samples in both feed (Fig. 14c) and normal direction (Fig. 14d) are almost the same for the same laser power. This is because the laser scanning process is conducted based on parameters determined by the inversed control method [19] and this results in near-homogenous heating and hence, the residual stress profile is similar in both directions. It can also be validated by observing the low level of grain misorientation of LS samples (Fig. 13c), which indicates there are no mechanical loading; thus, only thermal loading dominates the residual stress generation. However, the LAMill and CMill are conveying different information that the residual stress distributions in the two directions are unequal because the milling process (mechanical loading) has a different impact on the feed and normal directions.
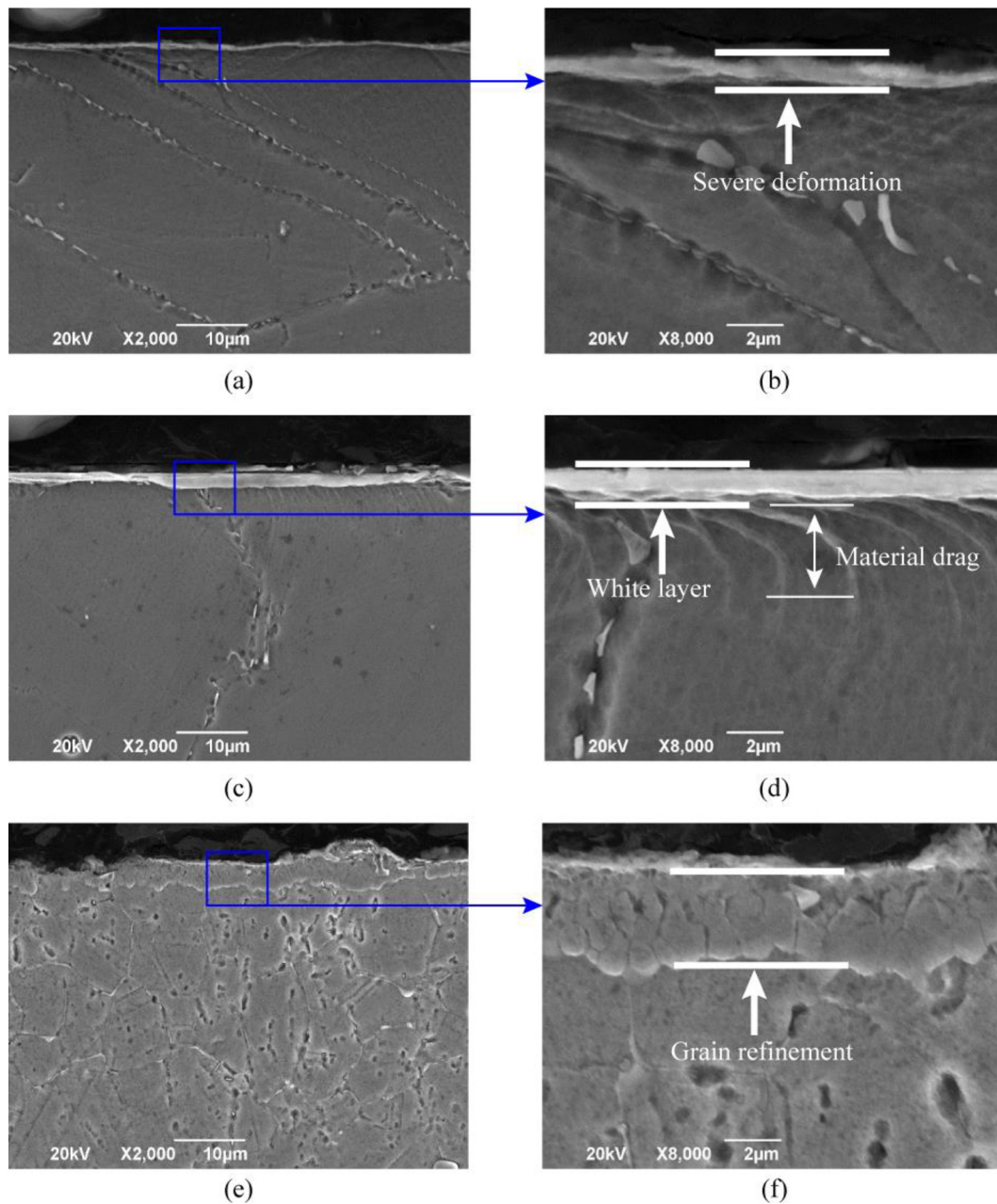
Fig. 11. SEM images (magnifications: ×2000 and ×8000) of the microstructure in the superficial layer generated by different processes: Severe plastic deformation layer (SPD) layer after LAMill process - (a) and (b); SPD layer after CMill - (c) and (d); re-solidified layer after LS - (e) and (f).

As a summary, it can be seen that at the very near top area (<100 μm) of the subsurface on LAMill samples (Fig. 14a and b) the residual stresses present a similar variation tendency (decreasing immediately) with those generated by CMill (Fig. 14c and d). This is because while the mechanical effect of the milling process penetrates only to shallow (100 μm - CMill effect) depths, the laser induced thermal effect can penetrate to deeper (~300 μm) into the superficial surface of workpiece. Hence, by hybridisation of CMill and LS processes, the total heat generated in LAMill process was increased when compared with individual machining generated heat (CMill) or laser scanning (LS). However, the generated mechanical compression loading (Fig. 14c and d) from milling cannot fully compensate this combined high thermal stress, which leads to a deeper impact on the machined workpiece with tensile effect, thus generating a complex residual stress distribution (Fig. 14a and b).

5.4. X-ray diffraction analysis

The XRD patterns (Fig. 15) are used to characterise the crystalline structures of generated workpiece surface by above processes (LAMill, CMill and LS), and they are measured on samples at different positions for several times to confirm repeatability. Apparent differences in relative peak sizes are found between LAMill/CMill and LS processes that broadening low peaks appear on CMill/LAMill machined workpieces and, as a clear comparison, the LS processed workpiece shows a sharp peak. It can be explained that the machining process will lead to severe plastic deformation and a recrystallised layer on the machined surface, making the crystallites smaller and then broadening the XRD peak; this can be linked/validated by observing the severe deformation layers presented in SEM and EBSD (Fig. 11 and Fig. 12). On the other hand, the non-uniform microstrain within crystals, which can be seen from the
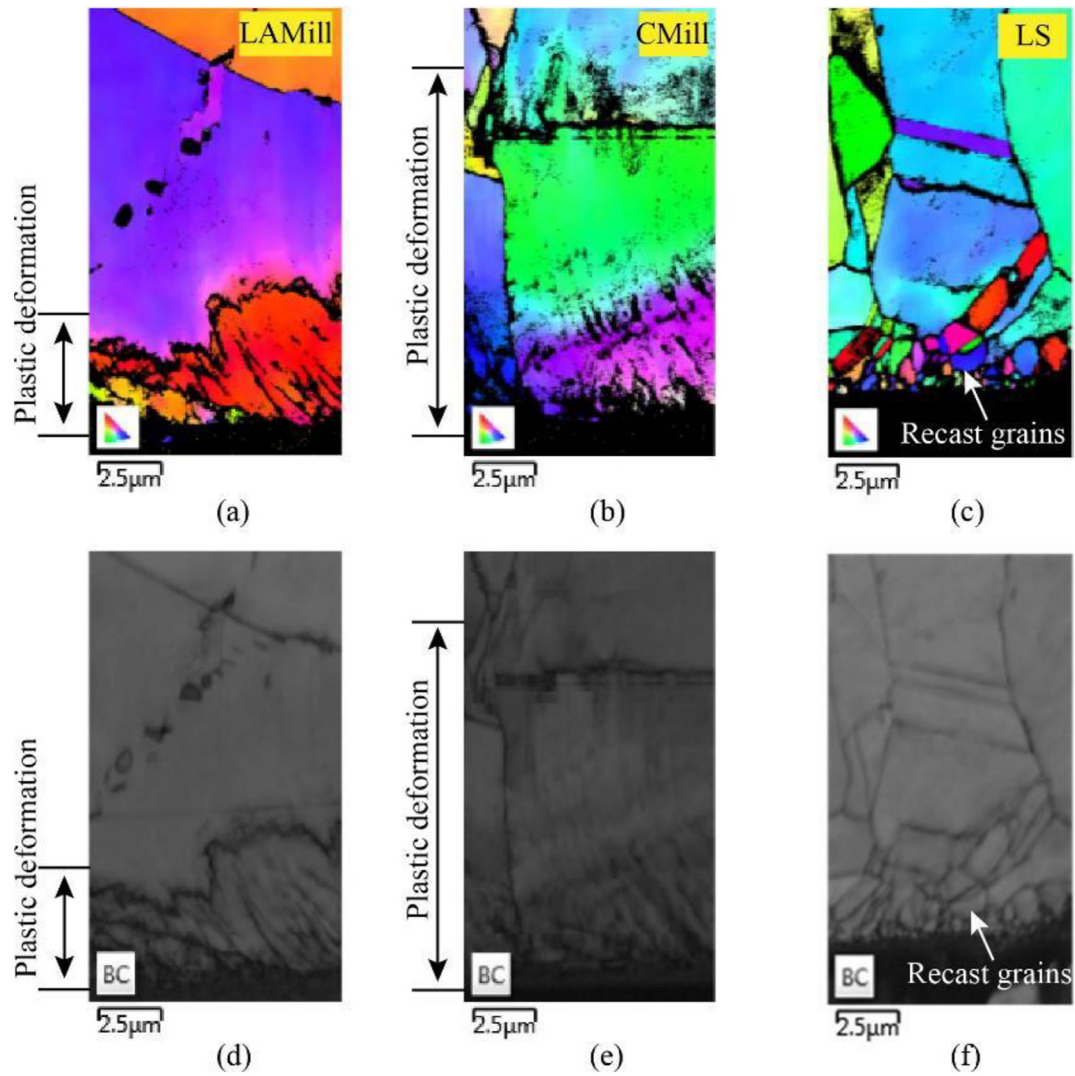
Fig. 12. Inverse pole figure and band contract images of superficial surface microstructure generated by different processes: LAMill-(a) and (d); CMill-(b) and (e); and LS-(c) and (f).

XRD Pawley fitting results (shown in the table of Fig. 15a), indicates that the LAMill has caused microstrain through plastic deformation at the level of 0.76%, which is around 5 times higher than the value (0.15%) in LS. Regarding the microstrain (1%) in CMill, it is even larger than the one in LAMill (0.76%), hinting that the CMill generated surface has experienced more significant deformation. This is because in LAMill
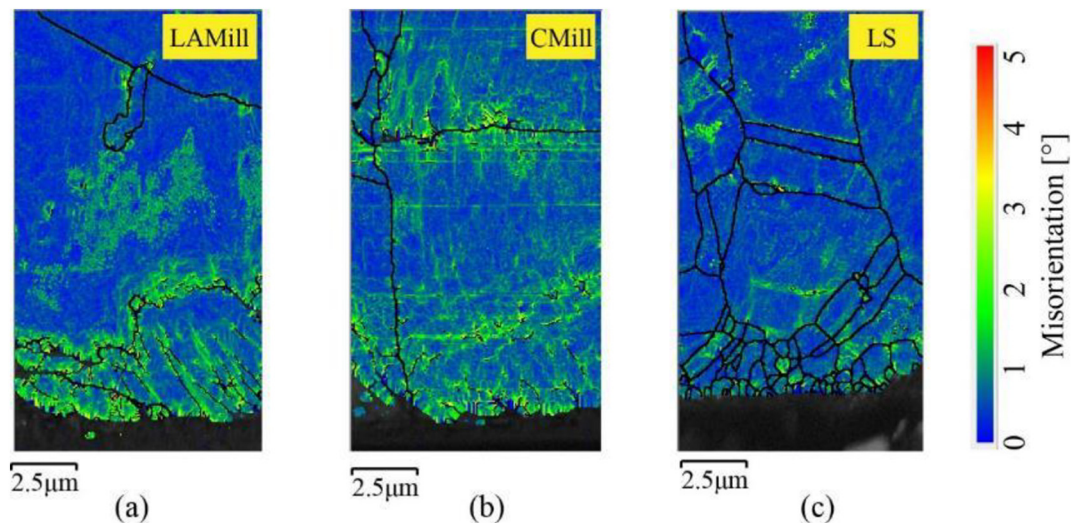
Fig. 13. Local misorientation map visualising the distribution of grain deformation for different processes: LAMill-(a), CMill -(b), and LS -(c).
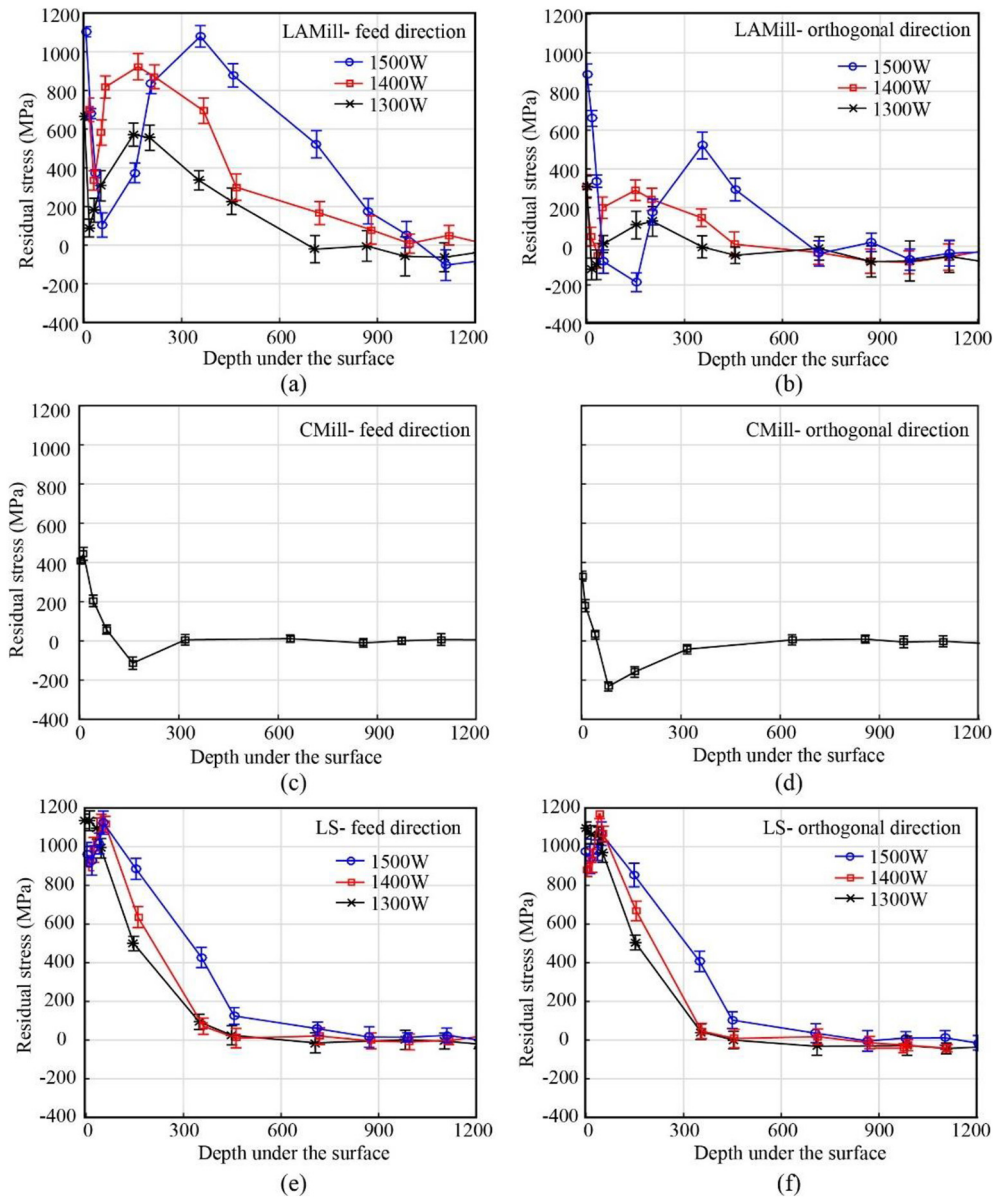
Fig. 14. Comparison of generated residual stresses by different processes: LAMill - feed direction (a); LAMill– orthogonal direction (b); CMill - feed direction (c); CMill – orthogonal direction (d); LS - feed direction (e); LS – orthogonal direction (f).

the workpiece material has been softened and less deformation is introduced on the surface, which can be validated from both the generated melt-like chips (Fig. 9d and Fig. 10d) and the thinner deformation depth in SEM and EBSD (Fig. 11d and Fig. 12b). This is also consistent with the peak shape in Fig. 15 (b) and (c) that the broaden extent for these three kinds of the workpiece has the trend that CMill>LAMill>LS.

Furthermore, it has also been noticed that the peaks from both LS and LAMill have slightly shifted to left (Fig. 15b-d) towards a lower angle compared with the peaks in CMill processed workpiece. The shift of peaks in the LAMill/LS machined surface indicates the increase of lattice plane distance of surface materials leading to observed tensile stress on surface (Fig. 14a and e), while this is obviously caused by the laser-induced high temperature. Moreover, the peak shifting of LS is more significant than LAMill process because the materials removal process has rapidly taken away lots of heat through the chips, therefore a higher thermal effect on the LS workpiece. This lattice parameter change is also associated with the release of the internal stress that caused the bending [30] in the acquired topography of machined workpiece (LS > LAMill>CMill). Although a variation of lattice parameters has

been observed, no change in crystal phase was evident, whereby a distorted peak shape can be found for each phase (e.g. the broad top of the 95.5° peak and 147° peak for LS in enlarging images of III and IV). This means that each this kind of peak is composed of several overlapping peaks close together, indicating the lattice variation after experiencing high temperature.

The broadening peak and larger microstrain, generated in CMill and LAMill when compared with LS process, is consistent with the severe plastic deformation on the corresponding surface, while the sharp peak in LS presents hardly any distortion as there is no plastic deformation. At the same time, the lattice parameter variation, displayed in peak shift and broadening, show the significant influence from the involved heat by laser and can be correlated to the workpiece bending caused by the residual stress distribution, as well as EBSD map.

5.5. Fatigue testing of the samples generated by different processes

Seen from the fatigue performance investigation of machined workpiece (Fig. 16), the minimum life (33,056 cycles) is found in LAMill
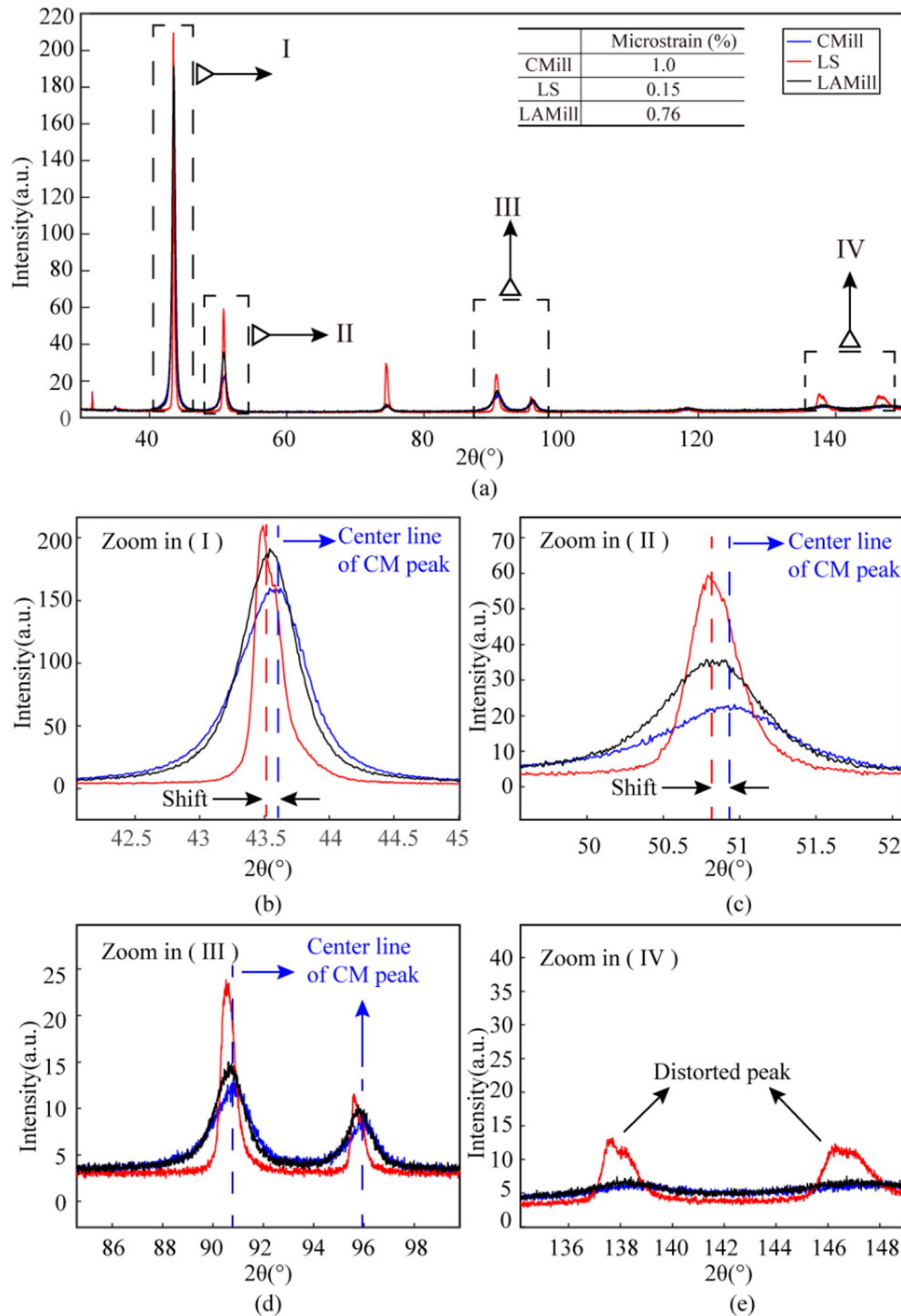
Fig. 15. X-ray diffraction diagrams of the workpiece surfaces generated by different processes: Overview of the acquired map at a large range (a); the enlarged images of indicated peaks (I, II, III, IV) for detailed analysis - (b), (c), (d) and (e).

samples, whereas the longest fatigue life (58,266 cycles in average) has been reached by the CMill samples. Although the LS samples show a slightly longer life (40,062 cycles) than the LAMill ones, it is still much less than the CMill generated workpiece. This could be backed up by the results from the residual stresses (Fig. 14) where it is noted that the LAMill has a more profound influence (tensile stress) in the machined workpiece. As the laser scanning process introduces a significant amount of heat, which has considerably influenced the residual stress distribution on LAMill and LS workpiece, and therefore, both of them

show shorter fatigue life compared with the conventional milling process.

SEM investigations on the fractured surfaces of the fatigue samples (Fig. 17) reveal the surface morphology difference in the texture and features of these regions to understand their failure modes. An apparent secondary crack is found in the deeper area below the free surface of the LAMill sample (30-40 μm from the top surface, Fig. 17a) while a cleavage fracture surface is presented in the rest of the areas. It is believed this secondary crack is caused by the residual tensile stress generated

under the machined surface during the LAMill process. This can be validated in the presented residual stress curves (Fig. 14a) that the LAMill processed samples preserve higher tensile stress at the deeper position because of the thermal influence from a combination of laser and machining heat.

Regarding the fractured surface of the samples generated by CMill, a clear crack initiating from the surface can be observed (Fig. 17d), while deeper bulk areas show cleavage fracture phenomenon. The distinct crack is probably caused by the machining induced grain refinement (white layer) and severe material deformation (material drag) in the superficial areas. Interestingly, upon inspection of the fracture region at LS samples, the fracture surface (Fig. 17e) appears to have distinct, well-defined planes which change orientation from grain to grain, indicating a crystallographic dependence. The smaller and intensive cleavage fractures in the near-surface area (Fig. 17f) are clearly correlated to the generated small grains by laser scanning, which has been revealed in above microstructure inspection.

It could be seen that the generated residual stress is determining the fatigue life of workpiece, while the microstructure (grain deformation, re-solidified grains) is contributing to the fracture surface morphology. Also, the results reveal the different fatigue modes caused by the difference in surface integrity: the noticeable crack in the deep area of LAMill sample initiates from the tensile residual stress; superficial grain alternation (white layer and material drag) contributes to the fracture on CMill generated workpiece; and the smaller grains (re-solidified layer) lead to cleavage fracture in LS samples.

6. Conclusions

While laser-assisted machining (LAM) has been reported as one of the most effective methods to improve the machinability of difficult-to-cut materials (e.g. Nickel based superalloy), the mechanism of surface integrity evolution and its influence on the material functional performance (e.g. fatigue life) of LAM have not been documented in detail before. To reveal the fundamental influence mechanism of LAM on the machined workpiece, the present study comprehensively investigates the laser-assisted milling (LAMill) by considering the workpiece surface integrity (residual stress distribution and microstructure alternation), generated chips and functional performance, while conventional machining and laser scanned only (i.e. without mechanical machining) samples, as a comparison, have been considered to support the understanding of the influence of the laser upon the workpiece properties resulted from LAMill. Detailed microstructural investigations of workpiece superficial layer provided an in-depth understanding of the influence mechanism of laser heating on the machined workpiece properties,

Fig. 16. Fatigue life cycles comparison for the different processes (conventional milling-CMill, laser-assisted milling-LAMill and laser scanning-LS); error bars represent fatigue life variation in repetition tests.

while the generated chips (morphology and microstructure) validates the significant thermal influence of laser on machining processes which in turn affects the workpiece surface integrity and functional performance. The main finding of the paper can be summarised as follows:

1. This study reveals the significant influence of the heat induced by the laser element in the LAMill upon the microstructure variation of both the chips and workpiece surface geometry and integrity. A melt-like layer has been observed on the free surface of LAMill generated chips due to the tremendous amount of heat introduced by using the laser, which has softened the workpiece material in front of the cutting tool. While apparent bending appears on the LS processed workpiece due to the thermal effect, it is interesting that this bending effect has not been eliminated by removing the softened layer in LAMill process; this is because of significant stresses induced by the laser heating on the machined workpiece. However, implementing the process on opposite surfaces (top and bottom), LAMill proved to be applicable to compensate for the thermal-induced distortions. Hence, it could be commented that this approach cannot be applied to "open" (e.g. prismatic) geometry parts while is applicable for the "close" ones (e.g. cylinders) as these deflections could be minimal due to the self-balance of the residual stresses.

2. The superficial surface microstructure investigations carried out by SEM and EBSD reveal the influence of LAMill process on the machined workpiece. It is interesting that the LAMill machined workpiece (using parameters selected by solving the inverse problem [19]) presents less damage in reference to grain alternation (white layer and material drag) and misorientation depth in the superficial surface when compared with CMill workpiece. This phenomenon is attributed to the 3D uniformly distributed laser heating effect resulting in a controlled softening depth of the workpiece which is subsequently removed by the machining process; this has been validated by putting in evidence the re-solidified layer on LS samples as well as the melt-like layer found in LAMill generated chips. Besides, the less broaden peaks of LAMill sample in XRD patterns also indicates that LAMill process presents a thinner grain refinement layer (white layer) compared with CMill one which showed broaden XRD peaks.

3. The present study reveals the generated complex residual stress distribution in LAMill machined workpiece and explains its formation mechanism. While the tremendously increased heat in LAMill leads to significant tensile residual stress on the workpiece surface, an interesting phenomenon is found in the deeper area: after the mechanical induced compressive residual stress (depth of 100 μm) induced by the machining process, high tensile stresses (up to 1100 MPa) appear again at increased depth (ca. 400 μm) beneath the surface. This is because the mechanical effect in the milling process cannot fully compensate the significant tensile stresses caused by the combined heat (induced by laser and machining as well) in LAMill process in deep areas of workpiece. The surface lattice parameters variation revealed by XRD diagram presents a shifting of the peaks to lower angles caused by laser heating in both LAMill and LS process, thus, validating the existing significant tensile stresses on the workpiece.

4. The evaluation of the functional performance and surface integrity reveal the advantages and drawbacks of LAMill process, which helps to optimise and progress its application. As reported in the fractography, the existing extensive tensile residual stress in the deep subsurface of LAMill sample leads to the noticeable crack, which attributes to the failure of LAMill machined workpiece. Although the fatigue life of LAMill machined test pieces is not as good as CMill generated ones, the LAMill proves advantageous in reducing cutting force and improvement of material removal rates. Therefore, the LAMill presents the potential for roughing machining but knowing the depths that is altered negatively (e.g. fatigue life), a subsequent finishing process or post-processed (e.g. shot peening) can be performed if needed.
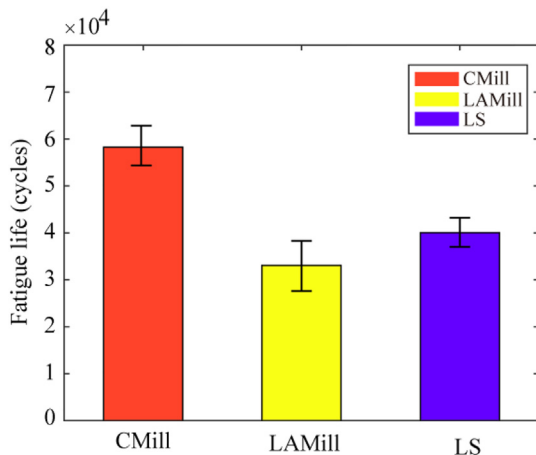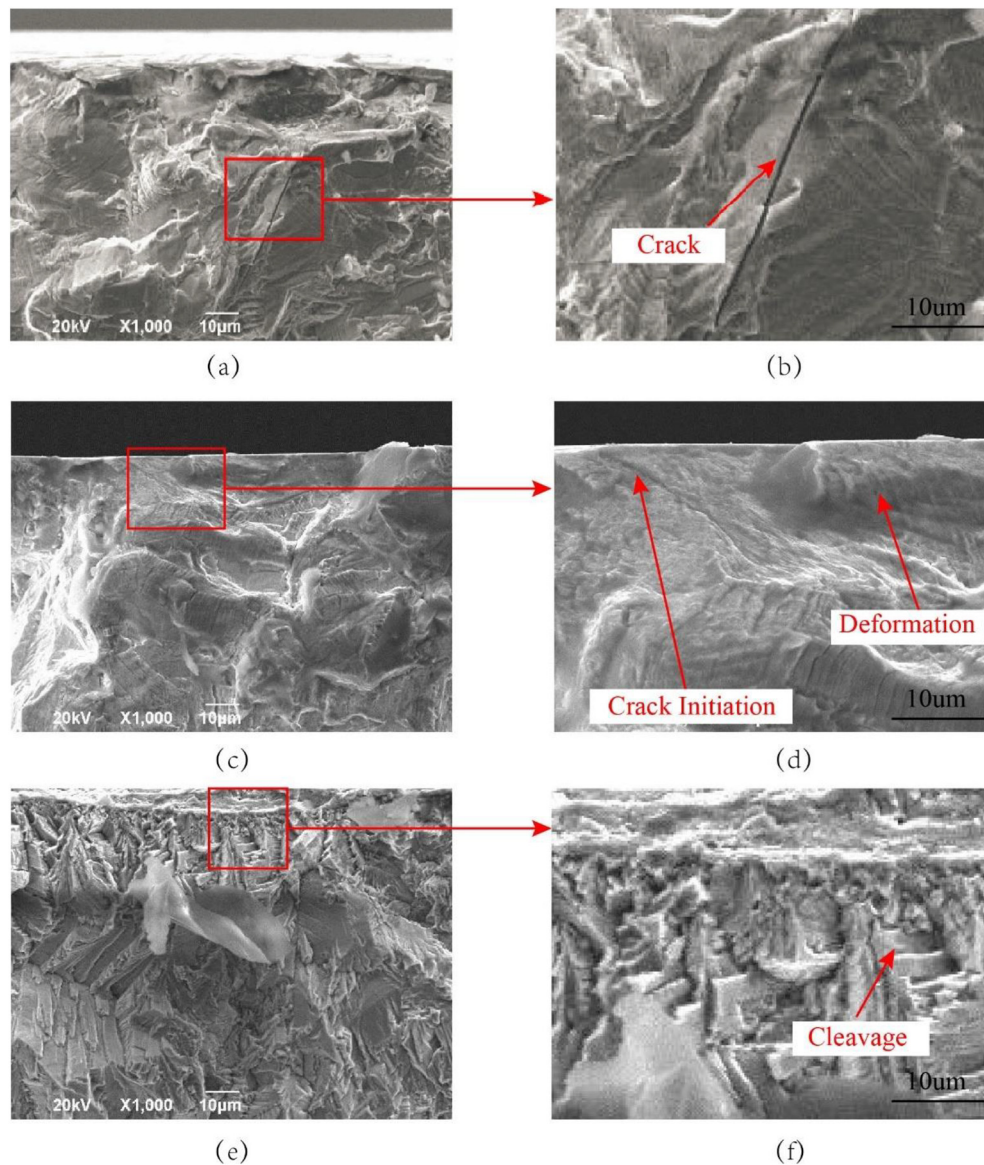
Fig. 17. Fracture surface morphology of samples after fatigue testing: LAMill-(a) and (b); CMill-(c) and (d); LS-(e) and (f).

Declaration of competing interests

The authors declare that they have no known competing financial interests or personal relationships that could have appeared to influence the work reported in this paper.

CRediT authorship contribution statement

Dongdong Xu: Conceptualization, Methodology, Investigation, Writing - original draft, Writing - review & editing, Validation. **Zhirong Liao:** Conceptualization, Methodology, Investigation, Writing - review & editing, Project administration, Validation. **Dragos Axinte:** Conceptualization, Supervision, Funding acquisition, Writing - review & editing. **Jon Ander Sarasua:** Writing - review & editing, Validation. **Rachid M'Saoubi:** Resources, Writing - review & editing. **Anders Wretland:** Funding acquisition, Writing - review & editing.

References

[1] A. Chamanfar, L. Sarrat, M. Jahazi, M. Asadi, A. Weck, A.K. Koul, Microstructural characteristics of forged and heat treated Inconel-718 disks, Mater. Des. 52 (2013) 791–800, https://doi.org/10.1016/j.matdes.2013.06.004.

[2] Z. Liao, D. Axinte, M. Mieszala, R.M. Saoubi, J. Michler, M. Hardy, On the influence of gamma prime upon machining of advanced nickel based superalloy, CIRP Ann. 67 (1) (2018) 109–112.

[3] O.G. Diaz, et al., The new challenges of machining Ceramic Matrix Composites (CMCs): review of surface integrity, Int. J. Mach. Tools Manuf. 139 (2019) 24–36.

[4] Y.C. Lin, K.K. Li, H. Bin Li, J. Chen, X.M. Chen, D.X. Wen, New constitutive model for high-temperature deformation behavior of inconel 718 superalloy, Mater. Des. 74 (2015) 108–118, https://doi.org/10.1016/j.matdes.2015.03.001.

[5] Z. Liao, et al., Grain refinement mechanism of nickel-based superalloy by severe plastic deformation - mechanical machining case, Acta Mater. 180 (2019) 2–14, https://doi.org/10.1016/j.actamat.2019.08.059.

[6] H. Zhang, K. Zhang, H. Zhou, Z. Lu, C. Zhao, X. Yang, Effect of strain rate on microstructure evolution of a nickel-based superalloy during hot deformation, Mater. Des. 80 (2015) 51–62, https://doi.org/10.1016/j.matdes.2015.05.004.

[7] D. Xu, et al., A novel method to continuously map the surface integrity and cutting mechanism transition in various cutting conditions, Int. J. Mach. Tools Manuf. 151 (2020), 103529. Apr https://doi.org/10.1016/j.ijmachtools.2020.103529.

[8] D. Xu, et al., A quick method for evaluating the thresholds of workpiece surface damage in machining, CIRP Ann. - Manuf. Technol 68 (1) (2019) 61–64, https://doi.org/10.1016/j.cirp.2019.03.015.

[9] Z. Liao, A. Abdelhafeez, H. Li, Y. Yang, O.G. Diaz, D. Axinte, State-of-the-art of surface integrity in machining of metal matrix composites, Int. J. Mach. Tools Manuf. 143 (2019) 63–91.

[10] S. Imbrogno, S. Rinaldi, D. Umbrello, L. Filice, R. Franchi, A. Del Prete, A physically based constitutive model for predicting the surface integrity in machining of Waspaloy, Mater. Des. 152 (2018) 140–155, https://doi.org/10.1016/j.matdes.2018.04.069.

[11] R.A.R. Rashid, S. Sun, G. Wang, M.S. Dargusch, An investigation of cutting forces and cutting temperatures during laser-assisted machining of the Ti–6Cr–5Mo–5V–4Al beta titanium alloy, Int. J. Mach. Tools Manuf. 63 (2012) 58–69.

[12] P. Dumitrescu, P. Koshy, J. Stenekes, M.A. Elbestawi, High-power diode laser assisted hard turning of AISI D2 tool steel, Int. J. Mach. Tools Manuf. 46 (15) (2006) 2009–2016.

[13] C.R. Dandekar, Y.C. Shin, J. Barnes, Machinability improvement of titanium alloy (Ti–6Al–4V) via LAM and hybrid machining, Int. J. Mach. Tools Manuf. 50 (2) (2010) 174–182.

[14] P.A. Rebro, Y.C. Shin, F.P. Incropera, Design of operating conditions for crackfree laser-assisted machining of mullite, Int. J. Mach. Tools Manuf. 44 (7–8) (2004) 677–694.

[15] Z. Pan, et al., Heat affected zone in the laser-assisted milling of Inconel 718, J. Manuf. Process. 30 (2017) 141–147.

[16] M. Anderson, R. Patwa, Y.C. Shin, Laser-assisted machining of Inconel 718 with an economic analysis, Int. J. Mach. Tools Manuf. 46 (14) (2006) 1879–1891.

[17] M.J. Bermingham, W.M. Sim, D. Kent, S. Gardiner, M.S. Dargusch, Tool life and wear mechanisms in laser assisted milling Ti–6Al–4V, Wear 322 (2015) 151–163.

[18] D. Cha, et al., Development of a novel system for in-situ repair of aeroengine airfoil via pulsed laser ablation, J. Manuf. Syst. 55 (March) (2020) 126–131, https://doi.org/10.1016/j.jmsy.2020.03.001.

[19] Z. Shang, et al., On modelling of laser assisted machining: forward and inverse problems for heat placement control, Int. J. Mach. Tools Manuf. 138 (2019) 36–50.

[20] M.A. Balbaa, M.N.A. Nasr, Prediction of residual stresses after laser-assisted machining of Inconel 718 using SPH, Procedia CIRP 31 (2015) 19–23.

[21] M.N.A. Nasr, M. Balbaa, H. Elgamal, Modelling machining-induced residual stresses after laser-assisted turning of steels, Advanced Materials Research, 996, 2014, pp. 622–627.

[22] Y. Tian, B. Wu, M. Anderson, Y.C. Shin, Laser-assisted milling of silicon nitride ceramics and Inconel 718, J. Manuf. Sci. Eng. 130 (3) (2008).

[23] P.J. Cheng, S.C. Lin, An analytical model for the temperature field in the laser forming of sheet metal, J. Mater. Process. Technol. 101 (1–3) (2000) 260–267.

[24] C. Multiphysics, Comsol Multiphysics User Guide (Version 4.3 a), COMSOL, AB, 2012 39–40.

[25] I.R. Kabir, D. Yin, N. Tamanna, S. Naher, Thermomechanical modelling of laser surface glazing for H13 tool steel, Appl. Phys. A Mater. Sci. Process. 124 (3) (2018) 260.

[26] Ż.A. Mierzejewska, Effect of laser energy density, internal porosity and heat treatment on mechanical behavior of biomedical Ti6Al4V alloy obtained with DMLS technology, Materials (Basel) 12 (14) (2019) 2331.

[27] W. Zhang, X. Wang, Y. Hu, S. Wang, Predictive modelling of microstructure changes, micro-hardness and residual stress in machining of 304 austenitic stainless steel, Int. J. Mach. Tools Manuf. 130–131 (2018) 36–48, https://doi.org/10.1016/j.ijmachtools.2018.03.008.

[28] A. Devillez, G. Le Coz, S. Dominiak, D. Dudzinski, Dry machining of Inconel 718, workpiece surface integrity, J. Mater. Process. Technol. 211 (10) (2011) 1590–1598.

[29] F. Pusavec, H. Hamdi, J. Kopac, I.S. Jawahir, Surface integrity in cryogenic machining of nickel based alloy Inconel 718, J. Mater. Process. Technol. 211 (4) (2011) 773–783.

[30] H.Q. Li, F. Ebrahimi, An investigation of thermal stability and microhardness of electrodeposited nanocrystalline nickel-21% iron alloys, Acta Mater. 51 (13) (2003) 3905–3913.